photonics

MDPI

Article

Decomposing Hong–Ou–Mandel Interference Under Realistic Sources: Intrinsic Overlap, Statistical Background, and Technical Noise

Lifeng Duan [1,2], Shuchen Guo [3], Yejun Xu [1,*] and Guoping Shi [4,*]

[1] Interdisciplinary Research Center of Quantum Information and Photoelectric Information (IRCQIPI), Chizhou University, Chizhou 247000, China
[2] Key Laboratory of Opto-Electronic Information Acquisitionand Manipulation, Ministry of Education, Anhui University, Hefei 230601, China
[3] Department of Intelligent Science and Technology, Hainan International College, Communication University of China, Lingshui 572400, China
[4] School of Mechanical and Electrical Engineering, Chizhou University, Chizhou 247000, China
* Correspondence: yejunxu@czu.edu.cn (Y.X.); sgp20062010@163.com (G.S.)

Abstract

Hong–Ou–Mandel (HOM) interference is a standard method for characterizing photon indistinguishability. However, in practical systems, the measured interference visibility is not solely determined by intrinsic spectral–temporal mismatch but can also be affected by photon-number statistics, multiphoton background, and technical noise. Here, we establish an observable-level framework for HOM interference in practical sources. Within this framework, under stationary-field and fixed-detection conditions, the measured coincidence rate is decomposed into a delay-dependent interference term and a stationary background term that is independent of the HOM interference. The former is described by an effective spectral overlap function $\mathcal{G}(\tau)$, while the latter mainly originates from source statistics and additive imperfections. This separation shows that the dip profile and intrinsic depth are governed by overlap-limited interference, whereas the observed visibility can be further degraded by statistical and external backgrounds. For single-photon and weak coherent-state inputs, $\mathcal{G}(\tau)$ represents the effective temporal–spectral mode overlap. For the stationary thermal field, its delay-dependent envelope can be related to the first-order temporal coherence function $g^{(1)}(\tau)$, whereas photon bunching contributes separately through $g^2(0)$. We further clarify that post-selection suppresses background and reveals intrinsic interference more directly but cannot improve the intrinsic spectral–temporal overlap. This framework provides a unified basis for distinguishing genuine indistinguishability loss from measurement-induced visibility degradation.

Keywords: HOM interference; visibility; spectral–temporal overlap

Check for updates

Received: 8 June 2026
Revised: 26 July 2026
Accepted: 14 August 2026
Published: 7 September 2026

Copyright: © 2026 by the authors. Licensee MDPI, Basel, Switzerland. This article is an open access article distributed under the terms and conditions of the Creative Commons Attribution (CC BY) license.

1. Introduction

Hong–Ou–Mandel (HOM) interference is one of the most fundamental phenomena of two-photon quantum interference in quantum optics [1,2]. It has become a standard means for characterizing photon indistinguishability. When two indistinguishable single photons are injected into a 50:50 beam splitter from two different input ports, quantum interference occurs between the two-photon probability amplitudes. As a result, the coincidence counts at the two outputs are strongly suppressed, which is named HOM dip [3,4]. Since its first demonstration, the HOM effect has not only deepened the understanding of fundamental

quantum interference but also has wide applications in various photonic quantum technologies, such as quantum communication, photonic quantum information processing [5,6], and distributed quantum networks [7,8]. In essence, the HOM dip provides an experimentally accessible signature of the indistinguishability of two optical excitations and therefore serves as a key observable in practical interference-based quantum protocols [2,3].

Under idealized conditions, the HOM interference visibility can reach unity. It is therefore regarded as a straightforward measurement of photon indistinguishability. In real experiments, however, this interpretation is generally incomplete. The measured coincidence dip is not determined only by intrinsic spectral–temporal overlap. Instead, it is usually affected by several factors acting together, including the photon-number statistics of the source, residual multiphoton contributions, imperfections in the mode structure, as well as unavoidable technical background noise [9,10]. As a result, the measured visibility cannot always be directly interpreted as a measurement of intrinsic indistinguishability [11,12]. On the other hand, even when the photons have perfect wave-packet overlap, the HOM interference visibility may still be reduced due to additional background noise introduced during the experiment. This distinction becomes increasingly important in practical systems involving non-ideal or different sources, where the measured HOM interference may contain both a genuine delay-dependent interference component and additional delay-independent contributions that do not originate from two-photon indistinguishability itself [8].

Therefore, how the visibility is modified under non-ideal conditions is a more essential question. In real experimental systems, the observed HOM visibility can hardly be taken as a direct measurement of intrinsic photon indistinguishability. It is usually affected by several factors at the same time, including spectral and temporal mismatch between the photons, the photon-number statistics of the source, as well as various kinds of technical background noise. These contributions are not independent; instead, they are mixed together in the total coincidence rate. Therefore, it is necessary to separate the genuine two-photon interference effect from the delay-independent background that is inevitably superimposed in the experiment. In this work, we address this issue by developing a unified observable-level description of HOM interference under realistic sources. We explicitly decompose the coincidence rate into a delay-dependent interference term and a delay-independent background. The intrinsic interference structure can be captured by an effective spectral overlap function, denoted as $G(\tau)$. This definition has a clear physical meaning in different situations. For two-photon interference between single-photon states and coherent states, $G(\tau)$ naturally reduces to the familiar wave-packet overlap. In contrast, when a thermal state is involved, $G(\tau)$ is more appropriately described, at the observable level, by the first-order temporal coherence function. Although the underlying physics is different, the same formal structure can still be maintained. Within this picture, the experimental HOM dip is understood as a joint result of intrinsic spectral overlap, photon-number statistics, and external noise.

2. Theoretical Model

In this section, we establish a compact theoretical framework to describe two-photon interference between two independent sources. We adopt a semiclassical description based on intensity correlations, which provides a direct connection to measurable quantities for weak classical fields (e.g., coherent and thermal states). Importantly, this description is used at the level of observable photon-number statistics and does not assume identical microscopic interference mechanisms for different quantum states. For quantum inputs such as single-photon Fock states, the same observable structure of the HOM dip can be recovered, although the underlying physical origin differs and a fully quantum mechanical

treatment is required. The two input fields are assumed to be statistically stationary during the HOM delay. The photon-number distributions, mean intensities, and equal-time second-order photon-number moments remain unchanged. The transmission loss, detection efficiency, coincidence window, and additive technical background are also assumed to be independent of the delay. We consider two independent fields injected into a balanced (50:50) beam splitter. The input fields are described by complex amplitudes $E_A(t), E_B(t)$, which represent stochastic optical signals with well-defined temporal envelopes. After the beam splitter, following the standard unitary transformation of a lossless 50:50 beam splitter, the output fields are given by [13]

$$E_C(t;\tau) = \frac{1}{\sqrt{2}}[E_A(t) + E_B(t-\tau)], \quad E_D(t;\tau) = \frac{1}{\sqrt{2}}[E_A(t) - E_B(t-\tau)]. \tag{1}$$

Here, τ denotes the relative arrival-time delay between the two input modes at the BS. It does not modify their marginal photon-number statistics. The experimentally measured coincidence rate is described in terms of the second-order intensity correlation function within the standard optical-coherence formalism [14]. It is written as

$$R(\tau) \propto \int_{\mathcal{W}} dt \, \langle I_C(t;\tau) I_D(t;\tau) \rangle, \tag{2}$$

where $\mathcal{W}$ denotes the fixed coincidence acquisition window. The coincidence rate can be expanded into several contributions by substituting the BS transformation into the above expression. For clarity, these terms are divided into two physically meaningful parts,

$$R(\tau) = R_{\text{bg}} + R_{\text{int}}(\tau), \tag{3}$$

where R_{bg} denotes the delay-independent background arising from the multiphoton components of the input states and $R_{\text{int}}(\tau)$ represents the delay-dependent interference contribution. $R_{\text{int}}(\tau)$ is decomposed into two parts: a statistical background arising from multiphoton components of the sources and an additional technical background due to experimental imperfections [15,16], which is introduced separately as R_{noise} in Equation (7).

To understand the observed HOM interference visibility, it is necessary to analyze both the background term R_{bg} and the interference term $R_{\text{int}}(\tau)$. The interference contribution originates from correlations between the two input fields. It can be expressed in terms of the mutual coherence function:

$$\Gamma_{AB}(\tau) = \langle E_A^*(t) E_B(t-\tau) \rangle. \tag{4}$$

It should be noted that this relation provides a semiclassical description for classical inputs with well-defined cross-correlations. More generally, we introduce $G(\tau)$ as an effective normalized temporal–spectral overlap function governing the delay-dependent interference envelope. For classical fields with a well-defined cross-correlation, it reduces to $G(\tau) = \frac{\Gamma_{AB}(\tau)}{\sqrt{\langle I_A \rangle \langle I_B \rangle}}$. For single-photon Fock-state inputs, $G(\tau)$ is the overlap between the two delayed single-photon modes. For phase-randomized weak coherent inputs, it represents the corresponding two-photon mode overlap rather than first-order phase coherence. For the stationary Gaussian thermal-field model considered here, the delay-dependent envelope can be related to the first-order temporal coherence function $g^1(\tau)$, whereas photon bunching and the same-source two-photon background are characterized separately by $g^2(0)$.

As we know, $|G(\tau)| \leq 1$, and $|G(0)|^2$ characterizes the intrinsic spectral–temporal overlap between the two inputs. The interference term is given by $R_{\text{int}}(\tau) \propto |\Gamma_{AB}(\tau)|^2$. For genuine two-photon quantum interference, there is an analogous dependence on the

overlap between the input states, although its origin lies in two-photon probability amplitudes rather than field correlations. In this sense, $|G(\tau)|^2$ can be interpreted as an effective observable measurement of indistinguishability across different sources. It shows that the depth and shape of the HOM dip are determined by the overlap between the two fields. When the two inputs are perfectly matched in both the spectral and temporal domains, the overlap is perfect, leading to the strongest suppression of coincidence events. Any mismatch in frequency, bandwidth, or arrival time between the two fields will inevitably lead to a reduction in the amplitude of $\Gamma_{AB}(\tau)$. As a result, the two-photon interference visibility is degraded. In addition to the overlap term, the overall coincidence level R_0 depends on the statistical properties of the input fields. For the weak-field case, the coincidence rate can be approximated as

$$R(\tau) \approx \langle I_A \rangle \langle I_B \rangle (1 - |G(\tau)|^2) + \Delta R, \tag{5}$$

where $\langle I_A \rangle$ and $\langle I_B \rangle$ denote the average intensities of the two input fields. ΔR is determined by the inputs' photon-number statistics, including mean photon numbers and $g_A^{(2)}(0)$ and $g_B^{(2)}(0)$, which remain constant during the HOM time delay. Hence, all the retained delay dependence is assigned to $G(\tau)$. Delay-dependent single-source intensity correlations, such as $g^{(2)}(\tau)$, nonstationary source fluctuations, delay-dependent transmission loss, and finite-gate clipping are not included in the present model. This approximation is adopted for weak stationary input fields. Apart from the photon-number contribution retained in ΔR, all the other high-photon-number contributions are neglected. The two-photon background included in ΔR remains constant when HOM delay is considered. For a weak coherent state, there is no excess fluctuation beyond Poissonian statistics; nevertheless, its finite two-photon probability contributes to the statistical coincidence background. For an ideal single-photon Fock state, the two-photon component is absent, and the corresponding two-photon background vanishes. For a thermal state, photon bunching enhances the two-photon probability and therefore increases the statistical coincidence background. Thus, the magnitude of ΔR is determined by the relevant two-photon probabilities of the input sources.

The ideal HOM interference visibility is defined as $V = \frac{R(\infty) - R(0)}{R(\infty)}$. Then the HOM interference visibility can be written as

$$V \approx \frac{\langle I_A \rangle \langle I_B \rangle |G(0)|^2}{\langle I_A \rangle \langle I_B \rangle + \Delta R}. \tag{6}$$

It shows that the interference visibility is determined by the competition between two effects: the numerator describes the intrinsic interference strength governed by field overlap, while the denominator reflects the total background arising from both independent intensities and statistical fluctuations. It is also valid under the same weak-field approximation and assumes stationary statistics of the input fields. Considering the weak-field approximation, we assume small mean photon numbers so higher-order intensity correlations are negligible and no detector-induced delay-dependent effects beyond $G(\tau)$. Thus, interference visibility reflects intrinsic interference strength relative to total effective background contribution terms included. Within the weak field approximation, each input state is considered to consist only of vacuum, single-photon, and two-photon components, while contributions involving three or more photons are neglected. The measured coincidence rate can therefore be written as

$$R_{\text{exp}}(\tau) \simeq R_{11}(\tau) + R_{20} + R_{02} + R_{\text{noise}}, \tag{7}$$

where $R_{11}(\tau)$ is the delay-dependent contribution from the $|1,1\rangle$, and R_{20} and R_{02} are delay-independent source contributions from $|2,0\rangle$ and $|0,2\rangle$, respectively. Blocking one input removes $R_{11}(\tau)$, but the two-photon component of the unblocked practical source may still produce coincidence events. Blocking both input arms removes all the source-dependent contributions, leaving only R_{noise}. For an ideal single-photon source with a vanishing two-photon component, the one-arm-blocked source-dependent background also vanishes. R_{noise} denotes an effective stationary experimental background combining detector dark counts, stray light, accidental coincidences, electronic noise, and timing-jitter-induced redistribution within finite coincidence windows. The measured visibility then becomes

$$V_{\text{exp}} = \frac{|\Gamma_{AB}(0)|^2}{\langle I_A\rangle\langle I_B\rangle + \Delta R + R_{\text{noise}}}. \tag{8}$$

This indicates that technical noise increases the effective background and reduces the observable visibility, even when the intrinsic overlap remains unchanged.

3. Numerical Simulations and Discussion

The numerical simulations are performed based on the theoretical framework introduced in Section 2. As discussed previously, the experimentally observed HOM interference is not governed by a single mechanism but rather results from the combined influence of several factors. First, the spectral–temporal overlap determines the HOM dip intrinsic shape. It reflects photon indistinguishability and the fundamental limit of the interference behavior. Second, under the stationary-field and fixed-detection assumptions, the photon-number statistics give rise to a stationary background component that does not depend on the delay. Third, technical noise further affects the measured visibility. To understand more clearly, we begin with the ideal case of two-photon interference, where only the spectral effect is included so that the basic mechanism can be clearly identified. On this basis, we then introduce realistic photon-number statistics to examine the background contributions. Finally, technical noise is taken into account, allowing us to assess the robustness of the interference under experimental conditions.

3.1. Ideal Two-Photon Interference

We begin with the idealized case in which the coincidence rate is only determined by the spectral overlap of the two input states. For single-photon wave packets, the normalized HOM coincidence probability can be written in terms of the temporal–spectral overlap function [17],

$$R_2(\tau) = 1 - |\mathcal{G}(\tau)|^2, \tag{9}$$

where $\mathcal{G}(\tau)$ denotes the effective spectral overlap function introduced in Section 2 and $R_2(\tau)$ is normalized such that $R_2(\tau \to \infty) = 1$. This expression shows that the HOM dip directly reflects the spectral indistinguishability of the two photons. Therefore, by analyzing the behavior of $R_2(\tau)$, one can extract the spectral information of the input fields. To systematically study this dependence, three representative scenarios are considered.

Figure 1 shows the two-photon coincidence probability for different combinations of spectral lineshapes with identical full width at half maximum (FWHM). When the two spectra have identical functional forms, the two-photon coincidence rate approaches zero at zero delay, indicating perfect overlap. However, when the spectral shapes differ between the two input fields, the minimum value of coincidence count is not zero. The results indicate that matching the spectral width is not enough to maximize the interference visibility. Instead, the detailed spectral structure plays a crucial role in determining the overlap.

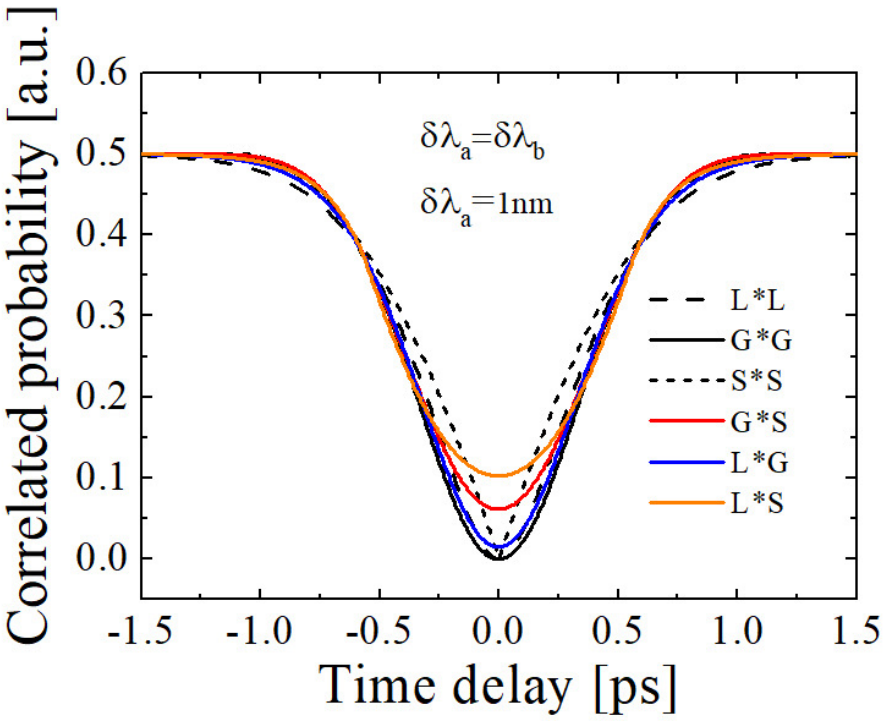


Figure 1. Two-photon coincidence probability $R_2(\tau)$ for different combinations of spectral amplitude functions. Panels show: Gaussian–Gaussian (G × G), Lorentzian–Lorentzian (L × L), sinc–sinc (S × S), Gaussian–Lorentzian (G × L), Gaussian–sinc (G × S), and Lorentzian–sinc (L × S). All the spectra are normalized and have the same full width at half maximum (FWHM) of 1 nm.

Figure 2 examines the effect of bandwidth mismatch for identical spectral lineshapes. Any deviation in the bandwidth ratio reduces the overlap at zero delay and modifies the temporal width of the HOM dip. This behavior reflects the fact that spectral indistinguishability requires matching both shape and bandwidth. A mismatch in bandwidth introduces distinguishability between the two photons, even when their spectral forms are identical.

Figure 3 considers the general case where both spectral shape and bandwidth are mismatched. Compared with the previous cases, the HOM dip exhibits stronger asymmetry and a more pronounced reduction in visibility. These results demonstrate that the HOM interference is governed by the full spectral overlap between the two inputs. The dip depth reflects the overlap magnitude, while the dip profile encodes detailed spectral information.

Beyond bandwidth and FWHM, HOM interference fundamentally depends on the full spectral overlap integral. Identical FWHM values do not guarantee high visibility as differing spectral shapes reduce overlap. Thus, spectral form mismatch critically affects indistinguishability. This is an effect that is overlooked by bandwidth-only analysis and requires careful spectral engineering for quantum applications. The above simulated cases correspond directly to several representative experimental scenarios. For example, Gaussian–Lorentzian and sinc-shaped spectra naturally arise in heterogeneous quantum emitter interference, such as quantum dot sources combined with SPDC photons. Bandwidth mismatch cases correspond to cavity-enhanced photon sources with different quality factors or spectrally filtered down-conversion processes. In addition, in remote-node quantum network experiments, independently optimized sources typically exhibit non-identical spectral envelopes and bandwidths, requiring spectral engineering or frequency conversion to achieve high-visibility interference. Therefore, the considered cases reflect realistic experimental constraints rather than purely idealized theoretical constructs.

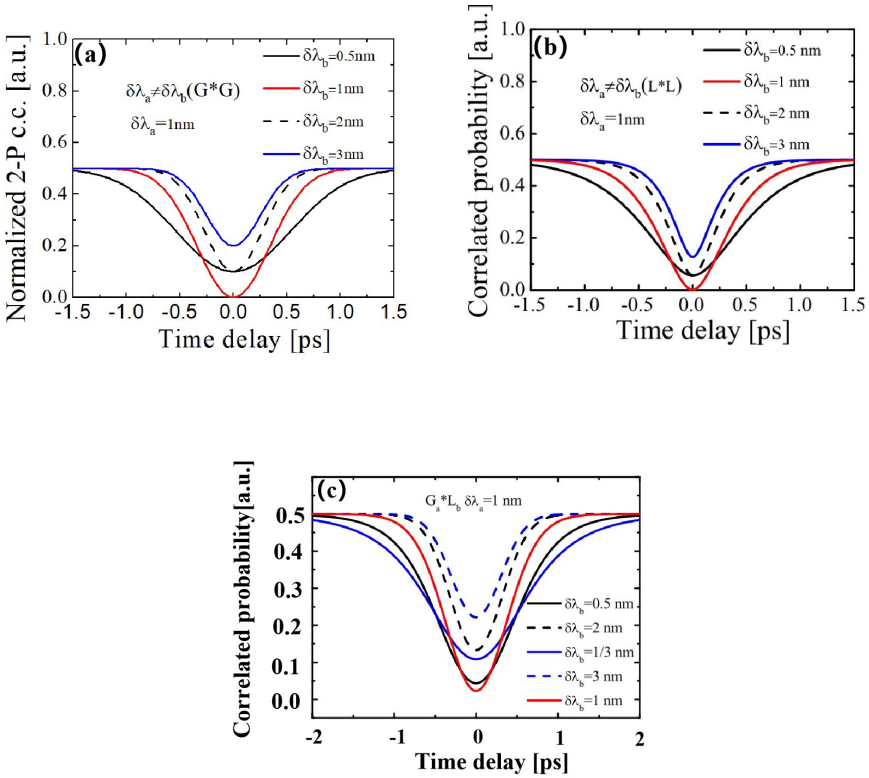


Figure 2. Two-photon coincidence probability $R_2(\tau)$ for identical spectral lineshapes with different bandwidth ratios. (**a**) Gaussian–Gaussian (G × G). (**b**) Lorentzian–Lorentzian (L × L). (**c**) Sinc–sinc (S × S). The FWHM of source *a* is fixed at 1 nm, while the FWHM of source *b* is scaled relative to it. All the spectra are normalized.

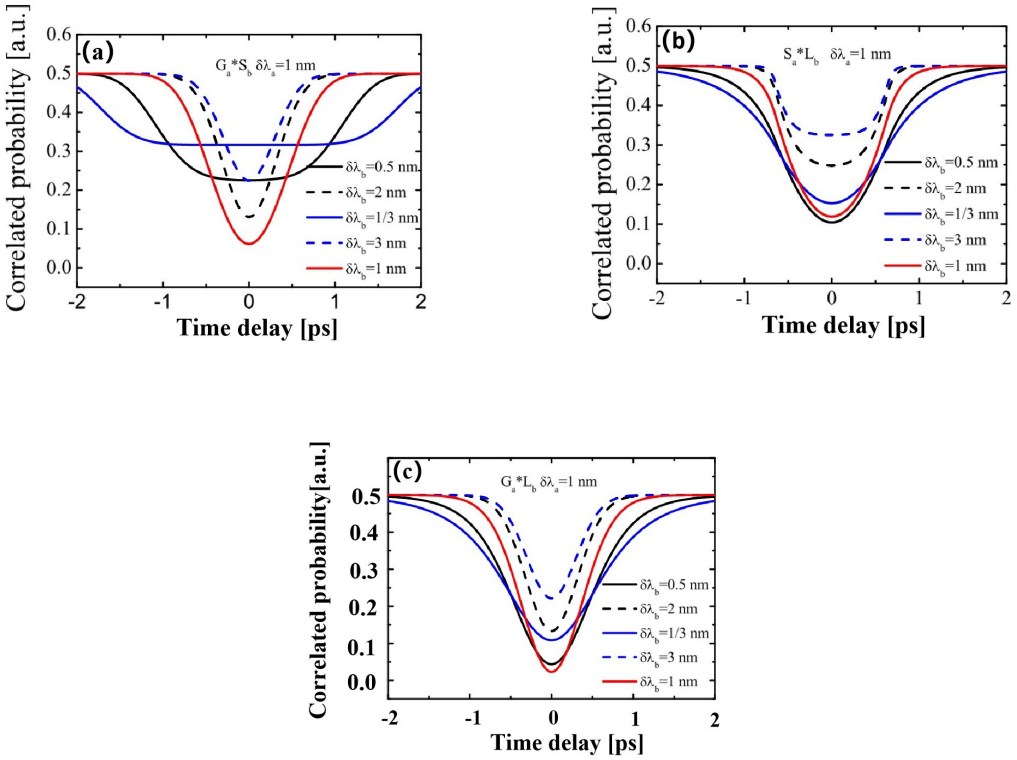


Figure 3. Two-photon coincidence probability $R_2(\tau)$ for mismatched spectral lineshapes and bandwidths. (**a**) Gaussian–sinc (G × S). (**b**) Lorentzian–sinc (L × S). (**c**) Gaussian–Lorentzian (G × L). The FWHM of source *a* is fixed at 1 nm. The FWHM of source *b* is varied as indicated in the plots. All the spectra are normalized.

3.2. Multiphoton Background and Post-Selection

We now consider realistic optical sources with nontrivial photon-number statistics. Here, $\mu_j \equiv \langle \hat{n}_j \rangle = \langle \hat{a}_j^\dagger \hat{a}_j \rangle (j = A, B)$ denotes the mean photon number per optical pulse of input source j. For a coherent state $|\alpha_j, \mu_j| = |\alpha_j|^2$. As discussed in Section 2, multiphoton components determine a stationary coincidence background through the photon-number distributions of the two inputs. This background is independent of the HOM time delay in the present model, whereas the delay dependence is contained in the overlap function $G(\tau)$. To clarify the physical origin of the observed interference patterns in Figures 4–6, it is helpful to explicitly separate three contributions: (i) the intrinsic spectral–temporal interference governed by the overlap function, (ii) the delay-independent background arising from multiphoton components of the input states, and (iii) the modification induced by post-selection, which effectively isolates the $|1,1\rangle$ subspace. Within this decomposition, they illustrate different combinations of these three effects under various source configurations.

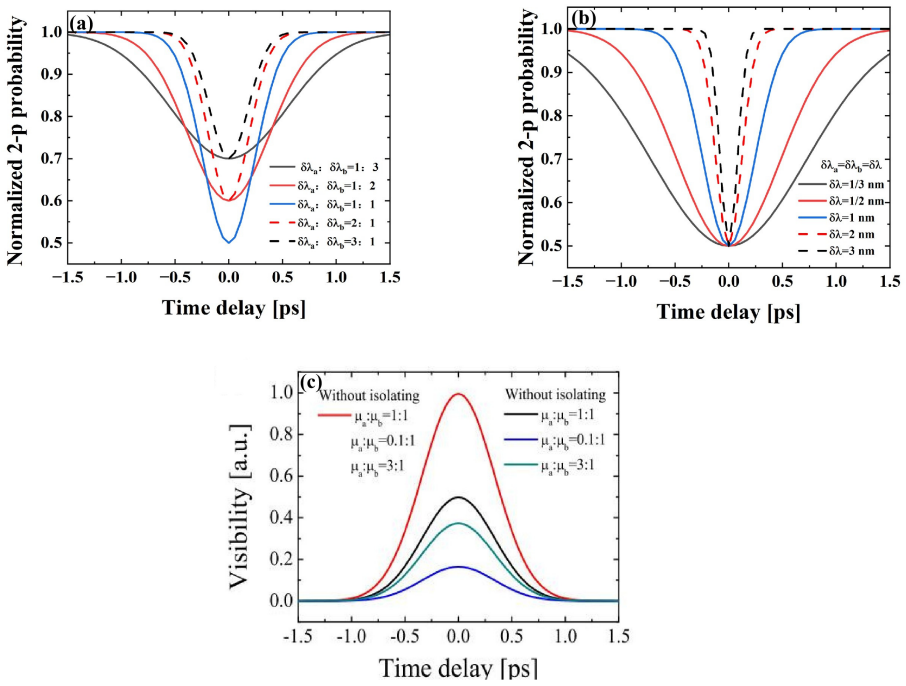


Figure 4. Interference between two weak coherent states with Gaussian distribution. (**a**,**b**) Normalized coincidence rate with different spectral width without isolating for $\mu_a = 0.1$ and $\mu_a/\mu_b = 1$. (**a**) Different spectral width ratio with fixed FWHM_b = 1 nm; (**b**) different spectral width with same ratio; (**c**) interference visibility as a function of time delay for identical spectra (FWHM_a = FWHM_b = 1 nm).

Figure 4 shows the HOM interference between two phase-randomized weak coherent states. As shown in Figure 4a,b, when the two input states have identical intensities and equal spectral widths, the maximum interference visibility is limited to 0.5. Once the spectral width ratio is not unity, the spectral overlap between the two inputs becomes imperfect, leading to a gradual reduction in visibility. This behavior indicates that spectral mismatch directly weakens the indistinguishability required for high-quality two-photon interference. The reduction in the maximum visibility from 1 to 0.5 mainly originates from the multiphoton components contained in weak coherent states [17,18]. These higher-order photon events do not participate in genuine two-photon interference but still contribute to the coincidence background at zero delay. Consequently, even under perfect spectral overlap, the coincidence probability cannot vanish completely, and the visibility is therefore fundamentally restricted to approximately 50% in the symmetric weak-excitation regime. To reveal the intrinsic interference contribution, post-selection can be employed to isolate

the two-photon events and suppress unwanted multiphoton background. This procedure modifies the effective detected statistics rather than the source itself. After post-selecting the $|1,1\rangle$ component and suppressing the same-source multiphoton components $|2,0\rangle$ and $|0,2\rangle$, the coincidence counts are predominantly determined by the genuine two-photon interference term. As shown in Figure 4c, the visibility can then approach unity for arbitrary intensity ratios, demonstrating that the degradation observed before post-selection mainly originates from statistical background rather than imperfect interference itself.

Figure 5 presents the two-photon interference between a weak coherent state and a single-photon state. As shown in Figure 5a,b, when the two input states possess identical spectral bandwidths, the interference visibility can ideally reach unity. However, the interference visibility decreases as the spectral bandwidth ratio deviates from unity owing to the reduced temporal–spectral overlap between the interfering photons. Unlike the interference between two phase-randomized weak coherent states, where residual multiphoton background fundamentally limits the visibility to 0.5, the presence of an ideal single-photon state strongly suppresses unwanted higher-order coincidence events, allowing complete destructive interference and therefore a maximum visibility of 1 [19,20]. Furthermore, after removing the two-photon contribution contained in the incident states, the remaining coincidence events originate entirely from indistinguishable single-photon interference. Consequently, as shown in Figure 5c, the interference visibility approaches unity for arbitrary intensity ratios of the input states.

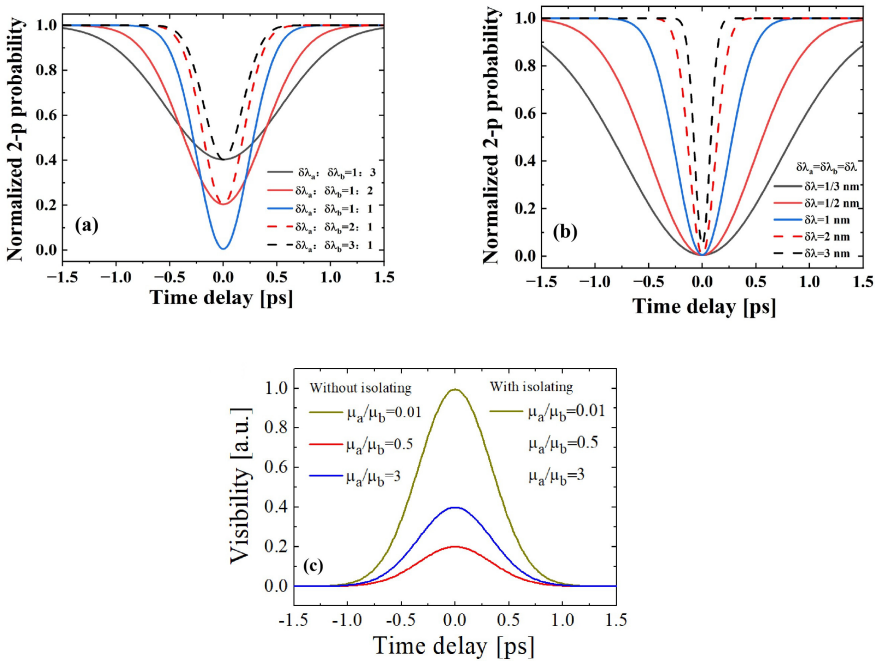


Figure 5. Interference between a weak coherent state and an ideal single-photon state with Gaussian spectra. (**a**,**b**) Normalized coincidence rate with different spectral width without isolating for $\mu_a = 0.01$ and $\mu_a/\mu_b = 0.01$. (**a**) Different spectral width ratio with fixed FWHM$_b$ = 1 nm; (**b**) different spectral width with same ratio; (**c**) interference visibility as a function of time delay for matched bandwidths (FWHM$_a$ = FWHM$_b$ = 1 nm).

Figure 6 illustrates the two-photon interference between a weak coherent state and a thermal state. Figure 6a,b show the coincidence probability as a function of time delay: (a) different spectral widths under the same spectral ratio and (b) different bandwidth ratios at a fixed spectral width. The interference visibility reaches maximum when the spectral ratio is the same, but it decreases when the spectral width ratio is mismatched because spectral mismatch reduces temporal overlap and increases distinguishability. Even with

the same spectral ratio, an excessively broad bandwidth can reduce the visibility due to shortened coherence time, temporal averaging, and enhanced multiphoton background. For this coherent-thermal interference, photon bunching in the thermal field further suppresses the observed visibility. However, after removing the two-photon components in the input states, the maximum visibility recovers to unity, as shown in Figure 6c.

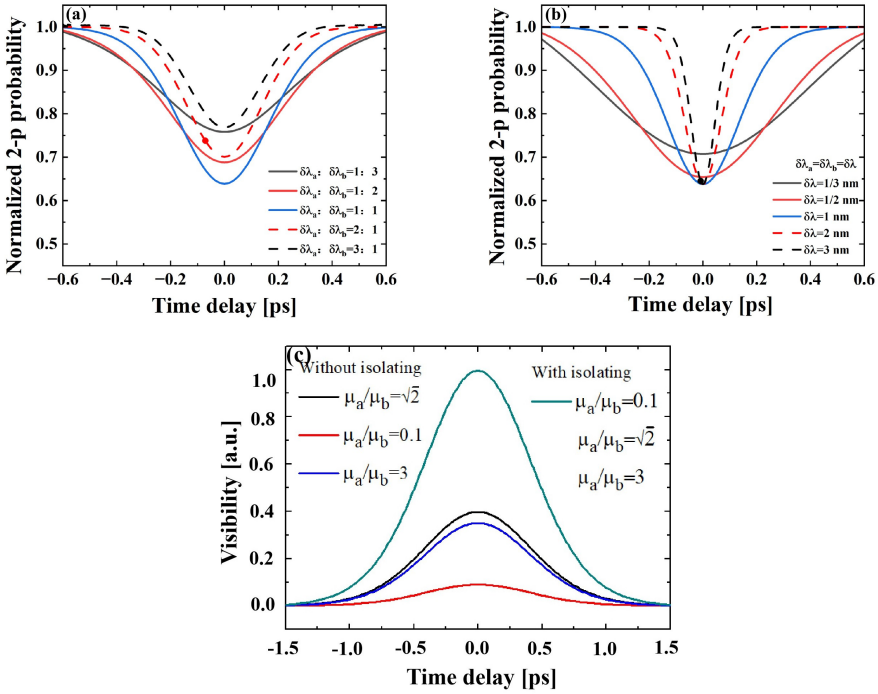


Figure 6. Interference between a weak coherent state with a Gaussian spectrum and a thermal state with a Lorentzian spectrum. (**a**,**b**) Normalized coincidence rate with different spectral width without isolating for $\mu_a = 0.01$ and $\mu_a/\mu_b = \sqrt{2}$. (**a**) Different spectral width ratio with fixed FWHM_b = 1 nm; (**b**) different spectral width with same ratio; (**c**) interference visibility as a function of delay for matched FWHM values (FWHM_a = FWHM_b = 1 nm).

It is emphasized that the observed visibility reduction in Figures 4–6 originates from three distinct mechanisms: (i) the delay-dependent $|1,1\rangle$ interference contribution governed by intrinsic spectral–temporal overlap $|G(\tau)|^2$, (ii) the delay-independent and source-dependent statistical background arising mainly from the same-source $|2,0\rangle$ and $|0,2\rangle$; and (iii) external technical noise R_{noise}, which may persist when both optical inputs are blocked. Post-selection modifies the detected event space by isolating the $|1,1\rangle$ subspace, thereby suppressing multiphoton-induced background. However, it does not alter the intrinsic overlap function $G(\tau)$ and therefore cannot overcome spectral distinguishability limits.

Beyond the statistical background discussed above, practical HOM measurements are further affected by technical imperfections that introduce an additional delay-independent coincidence background, denoted by R_{noise}. Unlike the statistical background, this residual contribution may remain when both optical input arms are blocked.

Figure 7a–c show that the observed two-photon visibility depends on system noise with different intensity ratios. For two weak coherent states, the visibility decreases relatively slowly as the noise level increases. This behavior arises because coherent states already exhibit a substantial delay-independent background from multiphoton components so that an additional constant noise term modifies the signal-to-background ratio more gradually. When a single-photon Fock state is involved, the intrinsic background is smaller on the single-photon side. As a result, the same level of technical noise produces a stronger relative reduction in visibility. For two-photon interference involving a thermal state, strong

photon-number fluctuations generate a large statistical background even in the absence of technical noise. In this case, the additional noise leads to a weaker relative change in the visibility, although the absolute visibility remains low. Overall, Figure 7 demonstrates that noise sensitivity is not intrinsic to the interference process itself but is determined by the signal-to-background ratio.

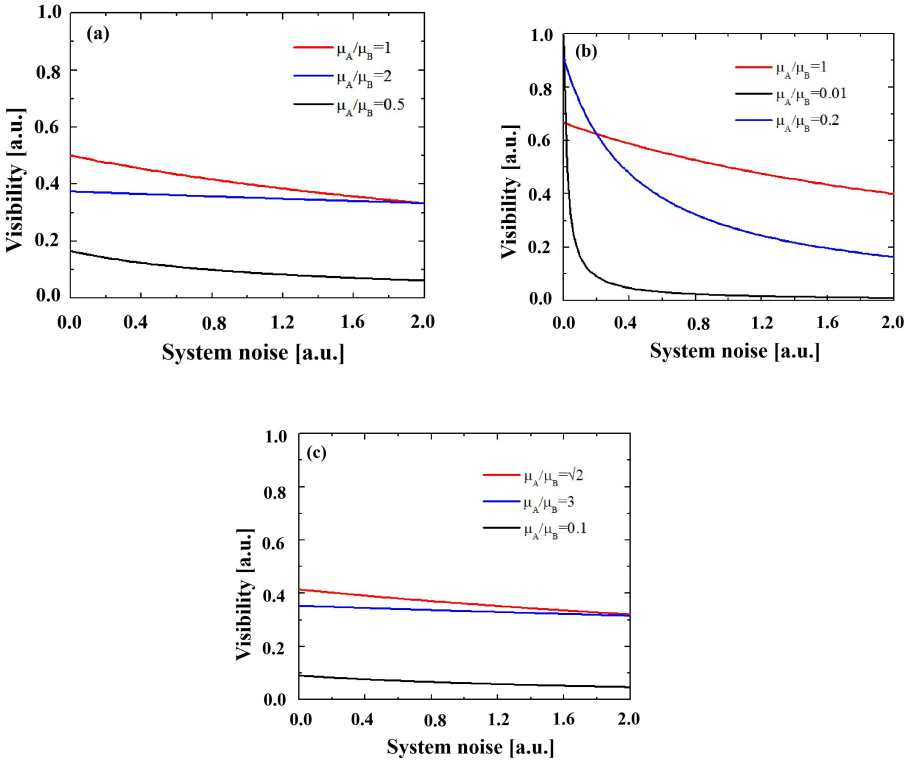


Figure 7. Interference visibility as a function of the system noise γ for matched FWHM values (FWHM$_a$ = FWHM$_b$ = 1 nm). (**a**) Two weak coherent states (coh–coh). (**b**) Weak coherent state and single-photon state (coh–Fock). (**c**) Weak coherent state and thermal state (coh–th).

Post-selection not only suppresses the multiphoton background but also modifies how the observed visibility responds to additional technical noise [9,11,12]. Figure 8 shows the post-selected visibility as a function of system noise for different intensity ratios. It is found that asymmetric input states exhibit improved robustness against noise, whereas symmetric weak fields lead to a faster degradation of visibility. This behavior can be understood from the scaling of the effective post-selected signal,

$$S \sim \mu_a \mu_b, \tag{10}$$

which determines the signal-to-background ratio in the presence of noise. In the asymmetric regime, the effective signal is primarily limited by the weaker inputs, while the residual background after post-selection remains relatively small. As a result, the same noise level produces a weaker relative reduction in visibility. In contrast, under symmetric weak excitation, the effective signal becomes comparable to the noise level, leading to enhanced noise sensitivity. This HOM interference contains three distinct components. Spectral overlap determines the structure of intrinsic interference. Photon-number statistics determine the level of the delay-independent background. Technical noise, such as detector dark counts and timing jitter, introduces an additional uniform background that further reduces the observable visibility [21,22]. Recent experiments have demonstrated that high-visibility HOM interference can still be achieved under realistic conditions through careful engineering of photon sources and detection systems [23,24]. Although post-selection

effectively suppresses the statistical background and enhances the HOM interference visibility, it cannot overcome the fundamental limit imposed by imperfect spectral overlap.

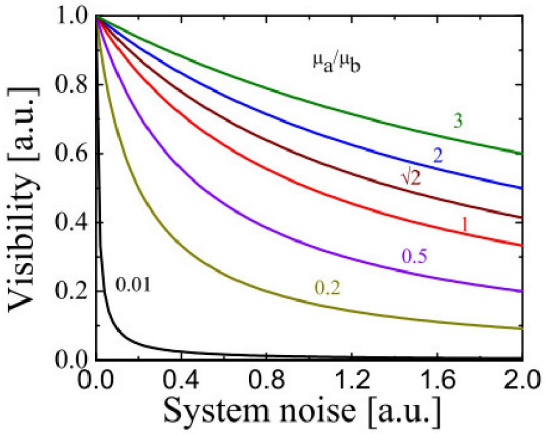


Figure 8. Post-selected interference visibility as a function of the system noise level γ for different intensity ratios and matched FWHM values ($FWHM_a$ = $FWHM_b$ = 1 nm).

4. Conclusions

We have established a model for HOM interference that links ideal two-photon interference with realistic optical sources. This includes photon-number statistics and technical noise. It is noted that the present framework provides a unified description of the experimentally observable coincidence signals rather than the underlying microscopic mechanisms. The results show that intrinsic HOM interference is fully determined by a single effective spectral overlap function, $\mathcal{G}(\tau)$, which governs both the dip profile and the fundamental visibility limit, $|\mathcal{G}(0)|^2$. Beyond this intrinsic limit, photon-number statistics introduce a source-dependent and delay-independent background through the same-source multiphoton components $|2,0\rangle$ and $|0,2\rangle$. Post-selection suppresses these components while retaining the $|1,1\rangle$ contribution that is responsible for HOM interference. In contrast, the residual technical background R_{noise}, including detector dark counts, electronic accidental coincidences, and residual stray light, may persist even when both optical inputs are blocked and further reduce the measured visibility. In summary, HOM interference in practical systems can be understood as arising from three contributions: spectral overlap determines the intrinsic interference, photon statistics determine the background and technical noise modifies the observed visibility [25]. These results provide guidance for optimizing interference with non-ideal sources and weak coherent light [26,27].

Author Contributions: Conceptualization, L.D. and Y.X.; methodology, L.D.; software, L.D. and S.G.; validation, G.S.; formal analysis, L.D. and Y.X.; investigation, L.D. and G.S.; data curation, L.D.; writing—original draft preparation, L.D.; writing—review and editing, L.D.; visualization, L.D. and S.G.; supervision, Y.X.; project administration, L.D.; funding acquisition, L.D. All authors have read and agreed to the published version of the manuscript.

Funding: This study was supported by the Open Research Fund of Key Laboratory of Opto-Electronic Information Acquisition and Manipulation (Anhui University), Ministry of Education (No. OEIAM202510), and the Priming Scientific Research Foundation for the Introduction of Talent at Chizhou University (No. CZ2025YJRC120).

Data Availability Statement: The data underlying the results presented in this paper are not publicly available at this time but may be obtained from the authors upon reasonable request.

Conflicts of Interest: The authors declare no conflicts of interest.

Abbreviations

The following abbreviations are used in this manuscript:

HOM	Hong–Ou–Mandel
G × G	Gaussian–Gaussian
L × L	Lorentzian–Lorentzian
S × S	Sinc–Sinc
G × L	Gaussian–Lorentzian
G × S	Gaussian–Sinc
L × S	Lorentzian–Sinc
FWHM	Full Width at Half Maximum

References

1. Mandel, L. Quantum effects in one-photon and two-photon interference. *Rev. Mod. Phys.* **1999**, *71*, S274. [CrossRef]
2. Hong, C.K.; Ou, Z.Y.; Mandel, L. Measurement of subpicosecond time intervals between two photons by interference. *Phys. Rev. Lett.* **1987**, *59*, 2044. [CrossRef] [PubMed]
3. Ghosh, R.; Mandel, L. Observation of nonclassical effects in the interference of two photons. *Phys. Rev. Lett.* **1986**, *59*, 1903. [CrossRef] [PubMed]
4. Ou, Z.Y. *Multi-Photon Quantum Interference*; Springer: Berlin/Heidelberg, Germany, 2007.
5. Pan, J.W.; Chen, Z.B.; Lu, C.Y. Multiphoton entanglement and interferometry. *Rev. Mod. Phys.* **2012**, *84*, 777. [CrossRef]
6. Slussarenko, S.; Pryde, G.J. Photonic quantum information processing. *Appl. Phys. Rev.* **2019**, *6*, 041303. [CrossRef]
7. Bernien, H.; Hensen, B.; Pfaff, W. Heralded entanglement between solid-state qubits. *Nature* **2013**, *497*, 86. [CrossRef] [PubMed]
8. Hoffet, F.; Lowinski, J.; Heller, L. Near-unity indistinguishability from independent nodes. *PRX Quantum* **2024**, *5*, 030305. [CrossRef]
9. Ollivier, H.; Thomas, S.E.; Wein, S.C.; Wenniger, I.M.d.; Coste, N.; Loredo, J.C.; Somaschi, N.; Harouri, A.; Lemaitre, A.; Sagnes, I.; et al. Hong-Ou-Mandel Interference with Imperfect Single Photon Sources. *Phys. Rev. Lett.* **2021**, *126*, 063602. [CrossRef] [PubMed]
10. Dangel, C.; Schmitt, J.; Bennett, A.J.; Müller, K.; Finley, J.J. Two-Photon Interference of Single Photons from Dissimilar Sources. *Phys. Rev. Appl.* **2022**, *18*, 054005. [CrossRef]
11. Dorfman, K.E.; Asban, S.; Gu, B. HOM interferometry and spectroscopy. *Commun. Phys.* **2021**, *4*, 49.
12. Fabre, N.; Felicetti, S. Parameter estimation with HOM interferometry. *Phys. Rev. A* **2021**, *104*, 022208. [CrossRef]
13. Campos R.A.; Saleh B.E.A.; Teich M.C. Quantum-mechanical lossless beam splitter: SU(2) symmetry and photon statistics. *Phys. Rev. A* **1989**, *40*, 1371–1384. [CrossRef] [PubMed]
14. Glauber R.J. The Quantum Theory of Optical Coherence. *Phys. Rev.* **1963**, *130*, 2529–2539. [CrossRef]
15. Patel, R.B.; Bennett, A.J.; Farrer, I. Two-photon interference of emission from remote quantum dots. *Nat. Photonics* **2010**, *4*, 632. [CrossRef]
16. McMillan, A.R.; Labonte, L.; Clark, A.S. Two-photon interference between disparate sources. *Sci. Rep.* **2013**, *3*, 2032. [CrossRef] [PubMed]
17. Legero, T.; Wilk, T.; Hennrich, M. Quantum beat of two single photons. *Phys. Rev. Lett.* **2006**, *96*, 023601. [CrossRef] [PubMed]
18. Rarity, J.G.; Tapster, P.R. Interference of weak coherent states. *J. Opt. B* **2005**, *7*, S171.
19. Santori, C.; Fattal, D.; Vuckovic, J. Indistinguishable photons from a single-photon device. *Nature* **2002**, *419*, 594. [CrossRef] [PubMed]
20. Somaschi, N.; Giesz, V.; Santis, L.D. Near-optimal single-photon sources. *Nat. Photonics* **2016**, *10*, 340. [CrossRef]
21. Hadfield, R.H. Single-photon detectors for optical quantum information. *Nat. Photonics* **2009**, *3*, 696. [CrossRef]
22. Eisaman, M.D.; Fan, J.; Migdall, A. Single-photon sources and detectors. *Rev. Sci. Instrum.* **2011**, *82*, 071101. [CrossRef] [PubMed]
23. Wang, H.; He, Y.; Li, Y. Boson sampling with 20 photons. *Nat. Photonics* **2019**, *13*, 770.
24. He, Y.M.; He, Y.; Wei, Y.J. Deterministic quantum dot photon source. *Nat. Nanotechnol.* **2022**, *17*, 1017. [CrossRef] [PubMed]
25. Flamini, F.; Spagnolo, N.; Sciarrino, F. Photonic quantum information processing. *Rep. Prog. Phys.* **2018**, *82*, 016001. [CrossRef] [PubMed]
26. Ojambati, O.S.; De, J.I.B.; Koenderink, A.F. Quantum interference control. *Optica* **2020**, *7*, 1577.
27. Chen, Y.; Zopf, M.; Keil, R. Quantum photonic circuits. *npj Quantum Inf.* **2021**, *7*, 1. [CrossRef]

Disclaimer/Publisher's Note: The statements, opinions and data contained in all publications are solely those of the individual author(s) and contributor(s) and not of MDPI and/or the editor(s). MDPI and/or the editor(s) disclaim responsibility for any injury to people or property resulting from any ideas, methods, instructions or products referred to in the content.